PRECISE STABILIZATION OF OPTICAL IMAGE AT A SPACE ASTRONOMICAL TELESCOPE BY A FINE PIEZO-DRIVER WITH PHYSICAL HYSTERESIS

Yevgeny Somov
Research Institute for Problems of Mechanical Systems Reliability
Samara State Technical University
Russia
e_somov@mail.ru

Sergey Somov
Research Institute for Problems of Mechanical Systems Reliability
Samara State Technical University
Russia
s_somov@mail.ru

Sergey Butyrin
Research Institute for Problems of Mechanical Systems Reliability
Samara State Technical University
Russia
butyrinsa@mail.ru

Abstract

Some problems on a nonius guidance, robust attitude control and long-time image stabilization of a large space astronomical telescope are considered. Elaborated methods for dynamic research under external and parametric disturbances, partial discrete measurement of the state, digital control of the gyro moment cluster and a fine piezo-driver with physical hysteresis, are presented.

Key words

Modeling, nonlinear dynamics, motion control

1 Introduction

The USA *Hubble Space Telescope* (*HST*), today the largest optical astronomical space telescope, has demonstrated the breadth of fundamental astrophysics that can be extracted from space-based observations. In the next two decades there will be made with ever more capable instruments and facilities. Today the Space Telescope Science Institute (*STSI*) develops the Advanced Technology Large Aperture Space Telescope (*ATLAST*) which is a NASA strategic mission concept study for the next generation of space observatory (see http://www.stsci.edu/institute/atlast). The *ATLAST* will have a primary mirror diameter in the 8m to 16m range that will allow to perform some of the most challenging observations to answer some of most compelling astrophysical questions.

The *ATLAST*-8m mission concept (Postmant *et al.*, 2008; Hopkins *et al.*, 2010) takes real advantage to launch an 8-meter monolithic primary mirror telescope to the second Sun-Earth Lagrange(L2) point in the 2020 decade. For this space observatory specific technical problems must be studied, included optical design; structural design and a vibration analysis; thermal analysis; launch vehicle performance and trajectory; spacecraft structure, propulsion, guidance, navigation, control and power systems; mass, power and cost budgets. The spacecraft performance capabilities and engineering design choices are directly traceable to science requirements:

pointing stability $1.6\ 10^{-3}$ arcsec;
maximum slew rate 60 degrees in 90 minutes;
maximum roll rate 30 degrees in 30 minutes;
maximum continuous inertial pointing 4500 minutes (9000 minutes goal);
momentum unloading interval 8 times in 22 days;
the Sun avoidance angle 60 degrees.

Additionally, the spacecraft (SC) employs a modular design philosophy to enable on-orbit servicing and replacement of subsystems. Assuming that servicing will occur on a regular basis, the spacecraft lifetime is 5 years with a goal of 10 years. All non-serviceable spacecraft components have a minimum design lifetime of 20 years. The SC solar array panels (SAPs) are sized to produce 11,160W of power, which includes 30 $\%$ margin at the end of a 10 year lifetime. Of this power, 2000W is for heating the primary mirror via electric heater panels to keep it at the desired 280K operational temperature. Under normal operations, 1600W is scavenged from the instruments. The SAPs are doubled gimballed to accommodate 240° slews (with $\pm 60^\circ$ Sun avoidance and $\pm 30^\circ$ on roll) for maintaining a balance on a solar pressure – principle external disturbance in the Sun-Earth L2 point. The SAPs are deployed on adjustable booms to provide solar pressure counter to the telescope tube, this balancing system can theoretically nullify all solar torques, providing unlimited observation times. The SAPs small angular replacements may be applied for permanent unloading an accumulated angular momentum (AM) of a gyro moment cluster (GMC) based on reaction wheels (RWs) or on control moment gyros (CMGs), but moreover large problems are arose on fine pointing stabi-

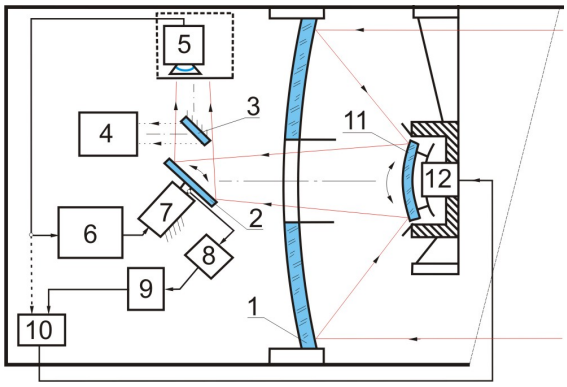

Figure 1. The scheme of the two-loop system for ultra-precise image motion stabilization: 1 — the main mirror; 2 — the near-focal optic compensator as the moving diagonal mirror; 3 — the fixed diagonal mirror; 4 — the light detector; 5 — the off-set fine image motion (position or/and velocity) sensor; 6, 9 and 10 — the micro-processors; 7 — the fine piezo-ceramic micro-drive; 8 — the fine sensor for the image motion compensator's 2 angular deviations; 11 — the optic compensator as the moving secondary mirror; 12 — the digital electro-mechanical micro-drive.

lization of the SC body into the inertial reference frame (IRF) if only the same GMC is applied for the SC attitude control.

A correct mathematical description of physical hysteresis is a *basic problem* for an *internal* friction theory (Sorokin, 1960; Panovko, 1960; Pisarenko, 1970; Palmov, 1976; Kochneva, 1979) and an *external Coulomb* friction theory (Dahl, 1968, 1976; Karnopp, 1985; Haessing and Friedland, 1991) with regard to the well-known *elastico-plastic* micro-deformations of materials. This problem is actual for electro-technique, electronics and a lot of natural science areas when there are need the *precise models* for electro-magnetic, dielectric and other types of *physical hysteresis*. The rigorous mathematical aspects for qualitative properties of general hysteresis models are represented in a number of research works (Krasnosel'skii and Pokrovskii, 1983). Presently new universal and *constructible* approach was elaborated for mathematical description of *physical hysteresis* based on using *set-valued* differential equation with discontinuous right-side and on a *shape* parametrization of a hysteresis relation. In this paper, some problems on guidance, robust attitude control and image motion stabilization of a large space astronomical telescope are considered, original nonius (vernier) approach is suggested for obtaining high accuracy of a long-time image motion stabilization by a fine piezo-driver with physical hysteresis.

2 Nonius Guidance of a Space Telescope

Conventionally, the SC attitude control system (ACS) have been designed in the form of a multi-functional system of combined control. Since it is the necessary for the closed loop to operate in the "reference memory" mode for long periods, this is the decisive criterion of efficiency. The principal meter for this loop has been represented by a strapdown inertial navigation system (SINS). Various meters for the SC body attitude and angular rate measurements have been applied to this loop: fine gyro and opto-electronic sensors, for example, a fine fixed-head star sensors with a wide field of view, which are intended for the correction of the gyro system. As far as ultra-precise image motion stabilization system is concerned (Somov and Dul'kin, 1975), the image, which is obtained with the main mirror (1) of the telescope in the light detector (4), has been precisely stabilized using two closed-loops, comprising the off-set fine image motion sensor (5), the fine sensor 8 for the image motion compensator's 2 angular deviations and micro-processors (6), (9) and (10). The movements of the optical compensators (the secondary mirror (11) and near-focal diagonal mirror (2)) is implemented by digital electro-mechanical (12) and piezo-ceramic (7) micro-drives. In result, there is obtained the nonius two-cascaded ACS:

I cascade — attitude guidance, navigation (by the SINS), gyromoment control (by the GMC) and angular stabilization of a space telescope body into the IRF with accuracy $3\sigma \approx 2$ arcsec;
II cascade — ultra-precise stabilization of an image position into the telescope focal plane with accuracy $3\sigma \approx 1.5\,10^{-3}$ arcsec by movements of the optical compensators on signals of the off-set fine image motion sensor.

Suggested nonius ACS, in cooperation with the solar pressure balancing system by the SAPs slow angular replacements for permanent unloading an accumulated AM of any GMC, may be applied for a long-time ultra-precise image motion stabilization.

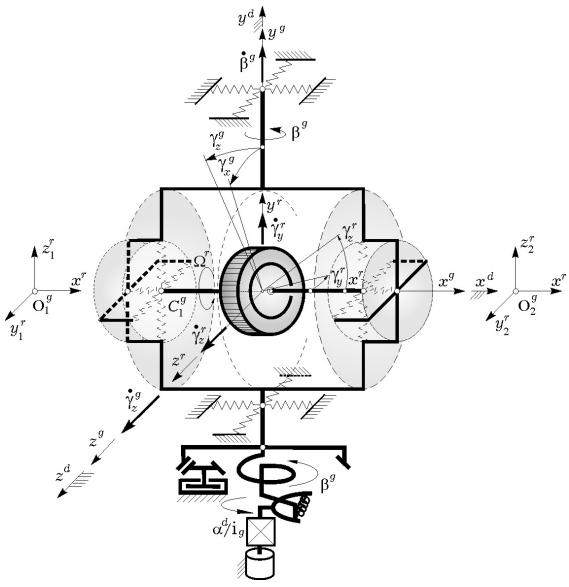

Figure 2. The scheme of a gyrodine

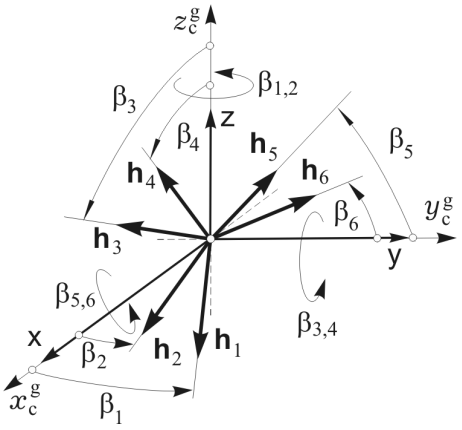

Figure 3. The scheme *3-SPE* by three collinear GD's pairs

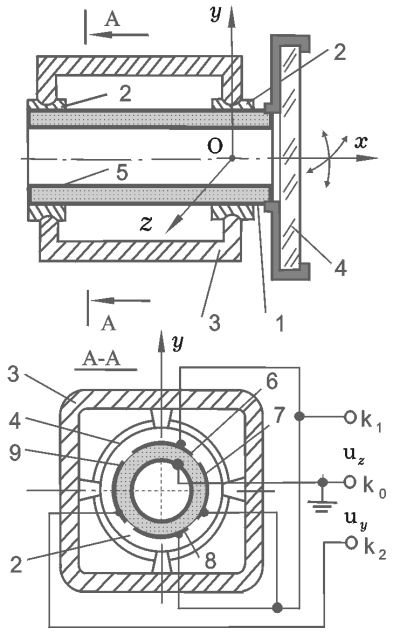

Figure 4. The scheme of the piezo-drive

3 Executed devices and systems

Increased requirements to information satellites (lifetime up to 10 years, exactness of spatial rotation manoeuvers with effective damping the SC flexible structure oscillations, robustness, fault-tolerance as well as to reasonable mass, size and energy characteristics) have motivated intensive development the GMCs based on excessive number of gyrodines (GDs) — single-gimbal control moment gyros, see Fig. 2. Collinear pair of two GDs was named as *Scissored Pair Ensemble* (*SPE*) in well-known original work *J.W. Crenshaw* (Crenshaw, 1973). Redundant scheme, based on six gyrodines in the form of three collinear GD's pairs, was named as *3-SPE*. Fig. 3 presents a simplest arrangement of this scheme into a canonical orthogonal gyroscopic basis $\mathrm{O}x_{\mathrm{c}}^{\mathrm{g}}y_{\mathrm{c}}^{\mathrm{g}}z_{\mathrm{c}}^{\mathrm{g}}$. By a slope of the GD pairs suspension axes in this basis it is possible to change essentially a form of the AM variation domain $\mathbf{S}$ at any direction.

The piezo-drive have a *tubular* construction with *bending* possibility at two orthogonal planes, see Fig. 4: a tubular piezo-ceramic element (PCE) 1, the elastic insulating spacers 2, a case 3 and an image motion compensator (IMC) 4 — a flat mirror. The PCE is freely attached to the case 3 on the borders at two orthogonal planes by spacers 2. The IMC 4 is rigidly connected to the end of the PCE 1 so that its reflecting plane is orthogonal to the PCE axis. The tubular PCE have 5 electrodes: general electrode 5 at its internal surface and 4 external electrodes 6–9 ordered along the PCE so that the symmetry planes of the opposite electrodes are mutually orthogonal (Somov, 1974). The PCE longitudinal parts have the *contrary* directions of *radial polarization* under the *opposite* electrodes. When a control voltage is appeared on the points $\mathsf{k}_1\&\mathsf{k}_0$ or $\mathsf{k}_2\&\mathsf{k}_0$ then due to a *reverse transverse* piezo-effect the PCE parts under electrodes 6&8 or respectively 7&9 are deformed in the *contrary* directions and therefore the PCE bends are happened at relevant planes. So, the tubular piezo-ceramic element is equivalent to the controlled 2-DOF *Hooke* hinge.

4 Mathematical Models

4.1 Model of Spacecraft Attitude Motion

Let us introduce the IRF $\mathbf{I}_{\oplus}$ $(\mathrm{OX_e^I Y_e^I Z_e^I})$, standard defined the body reference frame (BRF) $\mathbf{B}$ $(\mathrm{O}xyz)$ with origin in the SC mass center O, the optical telescope (sensor) reference frame (SRF) $\boldsymbol{\mathcal{S}}$ $(\mathrm{O}x^{\mathrm{s}}y^{\mathrm{s}}z^{\mathrm{s}})$ and the image field reference frame (FRF) $\boldsymbol{\mathcal{F}}$ $(\mathrm{O}_i x^i y^i z^i)$ with origin in center O_i of the telescope focal plane $y^i\mathrm{O}_i z^i$. The BRF attitude with respect to the IRF is defined by quaternion $\boldsymbol{\Lambda}_{\mathrm{I}}^{b} \equiv \boldsymbol{\Lambda} = (\lambda_0, \boldsymbol{\lambda}), \boldsymbol{\lambda} = (\lambda_1, \lambda_2, \lambda_3)$. Further the symbols $\langle\cdot,\cdot\rangle$, $\times$, $\{\,\cdot\,\}$, $[\,\cdot\,]$ for vectors and $[\mathbf{a}\times]$, $(\cdot)^{\mathrm{t}}$ for matrixes are conventional denotations. The GMC's AM vector $\boldsymbol{\mathcal{H}}$ have the form $\boldsymbol{\mathcal{H}}(\boldsymbol{\beta}) = \mathrm{h}_g \sum \mathbf{h}_p(\beta_p)$, there h_g is constant own AM value for each GD $p = 1, \ldots 6 \equiv 1 \div 6$ with the GD's AM unit $\mathbf{h}_p(\beta_p)$ and vector-column $\boldsymbol{\beta} = \{\beta_p\}$. Within precession theory of the control moment gyros, for a fixed position of the SC flexible structures with some simplifying assumptions and for $t \in \mathrm{T}_{t_0} = [t_0, +\infty)$ a SC angular motion simplest model is appeared as

$$\dot{\boldsymbol{\Lambda}} = \boldsymbol{\Lambda}\circ\boldsymbol{\omega}/2; \;\; \mathbf{A}^o\{\dot{\boldsymbol{\omega}}, \ddot{\mathbf{q}}\} = \{\mathbf{F}^{\omega}, \mathbf{F}^{q}\}, \qquad (1)$$

$$\begin{gathered}\boldsymbol{\omega}=\{\omega_i, i = x, y, z \equiv 1 \div 3\}; \mathbf{q}=\{q_j, j = 1 \div n^q\};\\ \mathbf{F}^{\omega} = \mathbf{M}^{\mathrm{g}} - \boldsymbol{\omega}\times\mathbf{G} + \mathbf{M}_d^o(t, \boldsymbol{\Lambda}, \boldsymbol{\omega}) + \mathbf{Q}^o(\boldsymbol{\omega}, \dot{\mathbf{q}}, \mathbf{q});\\ \mathbf{F}^{q}=\{-((\delta^q/\pi)\Omega_j^q\dot{q}_j + (\Omega_j^q)^2 q_j) + \mathrm{Q}_j^q(\boldsymbol{\omega}, \dot{q}_j, q_j)\};\\ \mathbf{M}^{\mathbf{g}} = -\dot{\boldsymbol{\mathcal{H}}} = -h_g\mathbf{A}_{\mathrm{h}}(\boldsymbol{\beta})\dot{\boldsymbol{\beta}};\;\; \mathbf{A}_{\mathrm{h}}(\boldsymbol{\beta}) = \partial\mathbf{h}(\boldsymbol{\beta})/\partial\boldsymbol{\beta};\end{gathered}$$

$$\mathbf{A}^o=\begin{bmatrix}\mathbf{J} & \mathbf{D}_q\\ \mathbf{D}_q^{\mathrm{t}} & \mathbf{I}\end{bmatrix};\;\; \begin{gathered}\mathbf{G} = \mathbf{G}^o + \mathbf{D}_q\dot{\mathbf{q}};\\ \mathbf{G}^o = \mathbf{J}\,\boldsymbol{\omega} + \boldsymbol{\mathcal{H}}(\boldsymbol{\beta}),\end{gathered}$$

vector-column $\mathbf{M}_d^o(\cdot)$ presents an external torque disturbance, and $\mathbf{Q}^o(\cdot), \mathrm{Q}_j^q(\cdot)$ are nonlinear continuous

functions. The GMC torque vector $\mathbf{M^g} = \mathbf{M^g}(\boldsymbol{\beta}, \dot{\boldsymbol{\beta}})$ is presented as follows:

$$\mathbf{M^g} = -\dot{\boldsymbol{\mathcal{H}}} = -h_g \mathbf{A}_{\rm h}(\boldsymbol{\beta})\, \mathbf{u}^{\rm g}; \quad \dot{\boldsymbol{\beta}} = \mathbf{u}^{\rm g}, \qquad (2)$$

$\mathbf{u}^{\rm g}=\{{\rm u}^{\rm g}_p\}$, ${\rm u}^{\rm g}_p(t) = a^{\rm g}\,{\rm Zh}[{\rm Sat}({\rm Qntr}(u^g_{pk}, d^g), \bar{\rm u}^{\rm m}_{\rm g}), T_u]$ with constants $a^{\rm g}$, d^g, $\bar{\rm u}^{\rm m}_{\rm g}$ and a control period $T_u = t_{k+1} - t_k$, $k \in \mathbb{N}_0 \equiv [0, 1, 2, ...)$; discrete functions $u^g_{pk} \equiv u^g_p(t_k)$ are outputs of digital nonlinear control law (CL), and functions ${\rm Sat}(x, a)$ and ${\rm Qntr}(x, a)$ are general-usage ones, while the holder model with the period T_u is such: $y(t) = {\rm Zh}[x_k, T_u] = x_k\, \forall t \in [t_k, t_{k+1})$. At given the SC body angular programmed motion $\boldsymbol{\Lambda}^p(t)$, $\boldsymbol{\omega}^p(t)$, $\boldsymbol{\varepsilon}^p(t) = \dot{\boldsymbol{\omega}}^p(t)$ with respect to the IRF $\mathbf{I}$ during time interval $t \in {\rm T} \equiv [t_{\rm i}, t_{\rm f}] \subset {\rm T}_{t_0}$, $t_{\rm f} \equiv t_{\rm i} + T$, and for forming the vector of corresponding continuous control torque $\mathbf{M^g}(\boldsymbol{\beta}(t), \dot{\boldsymbol{\beta}}(t))$ (2), the vector-columns $\dot{\boldsymbol{\beta}} = \{\dot{\beta}_p\}$ and $\ddot{\boldsymbol{\beta}} = \{\ddot{\beta}_p\}$, $p = 1 \div 6$, must be component-wise module restricted:

$$|\dot{\beta}_p(t)| \le \bar{\rm u}_{\rm g} < \bar{\rm u}^{\rm m}_{\rm g}, \;\; |\ddot{\beta}_p(t)| \le \bar{\rm v}_{\rm g}, \; \forall t \in {\rm T}, \qquad (3)$$

where values $\bar{\rm u}_{\rm g}$ and $\bar{\rm v}_{\rm g}$ are constant.

Model of a space telescope takes into account (Somov, 2000): the controlled motion of the SC mass center; the spatial angular motion of the SC as a rigid body; movements of flexible SAPs and antennas; the GD movements into the GMC scheme, see Fig. 3, moreover the model of each gyrodine describes the nonlinear dynamics of the gyro-rotor's 5-DOF ball bearing suspension, see Fig. 2, the proper gyro-rotor rotation dynamics with regard to its *static* and *dynamic* unbalance, the flexibility of gyro-shell's ball bearings, the flexibility and kinematic defects in the gear, the dynamics of stepping motor and an electromagnetic damper on the gyrodine precession axis that takes into account the dry friction torque; the GMC fixation on the SC body by means of a vibration-absorbing frame; external torques, including ones by solar pressure; the flexible-viscous fixation of the optical telescope structure on the SC body by a vibration-absorbing frame, taking into account a nonlinear dynamics of the digital electro-mechanical micro-drive (12) with a precision screw gear and the fine piezo-ceramic micro-drive (7), see Fig. 4; operation of the system's meter elements taking into account the proper dynamics of these devices, their nonlinearities, the digital forming output signals, the discrete noise influences and a delay with respect to the main cycle of the onboard computer operation, including that for the fine opto-electronic image motion sensor (5) and the fine sensor (8), see Fig. 1.

4.2 General Model of Physical Hysteresis

As well known, fundamentally two types of the hysteresis relations are singled out in any physical medium: with index of a *limiting static loop* in negative direction (clockwise, Fig. 5 *a*, type $\mathcal{A}$) and with index

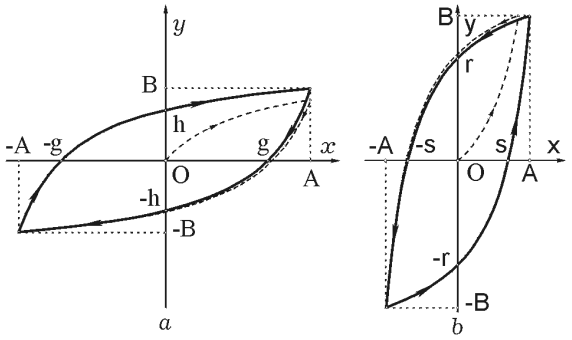

Figure 5. The types of physical hysteresis

of this loop in positive direction (counter-clockwise, Fig. 5 *b*, type $\mathcal{B}$). It is very important to distinguish a physical meaning of the arguments x and y for hysteresis function $y = F_h(\cdot, x)$. For example, *elastico-plastic* micro-deformations (Palmov, 1976) in an *internal* friction theory under notation $x = \varepsilon$ (mechanical deformation) and $y = \sigma$ (mechanical strength) are represented by the type $\mathcal{A}$ hysteresis relation. In an *external* friction theory the elastico-plastic micro-deformations have also such type hysteresis relation, if a variable x is a small line or angular displacement, and a variable y is respectively a friction force or torque, as in famous *Dahl*-type solid friction model (Dahl, 1968).

Ferro-magnetic hysteresis is presented by a $\mathcal{B}$-type multi-function (see Fig. 5 *b*), if in the capacity of a forcing variable there is assumed $\mathsf{x} = H$ (magnetic field strength) and as a output variable — function $\mathsf{y} = B$ (magnetic displacement). For piezo-ceramic materials a *dielectric* hysteresis have also such type hysteresis relation, if as a forcing function there is assumed a variable $\mathsf{x} = E$ (electric field strength), and as a output variable — function $\mathsf{y} = P$ (polarization of a segneto-electric material).

The $\mathcal{A}$-type hysteresis relation $y = F_h(\cdot, x)$,Fig. 5 *a*, is transformed in hysteresis function $\mathsf{y} = \Phi_h(\cdot, \mathsf{x})$ of the type $\mathcal{B}$, see Fig. 5 *b*, (e.g. in the form $x = \Phi_h(\cdot, y)$) by the "mirror reflection" respect to an ordinate (the axis y) with a next rotation of obtained image on the angle $-\pi/2$ (90° clockwise), and also renaming the coordinate axes as $\mathsf{x} = y$ and $\mathsf{y} = x$. Moreover, for the *model limiting hysteresis loop* the coordinates of characteristic points in Fig. 5 are transformed in such obvious way: $\mathsf{B} = \mathrm{A}$; $\mathsf{A} = \mathrm{B}$ and $\mathsf{r} = \mathrm{g}$; $\mathsf{s} = \mathrm{h}$. This method is well known, often is used, for example in the *internal* friction theory (Kochneva, 1979), and permits to investigate only *one type* of hysteresis relation, in the capacity of which later on is assumed the type $\mathcal{A}$.

Let $x(t)$ is a real continuous and piecewise-differetiated function for $t \in {\rm T}_{t_0} \equiv [t_0, +\infty)$. Let there be the values $\check{x}_\nu = x(t_\nu)$ of the function in the time moments t_ν, $\nu \in \mathbb{N}_0 \equiv [0, 1, 2, \cdots)$, when the *last* changing *sign* of a speed $\dot{x}(t)$ (a derivative of $x(t)$ with respect to time t) was happened, e.g.

$$\check{x}_\nu \equiv x(t_\nu)|t_\nu : {\rm Sign}\dot{x}(t_\nu + 0) \ne {\rm Sign}\dot{x}(t_\nu - 0). \quad (4)$$

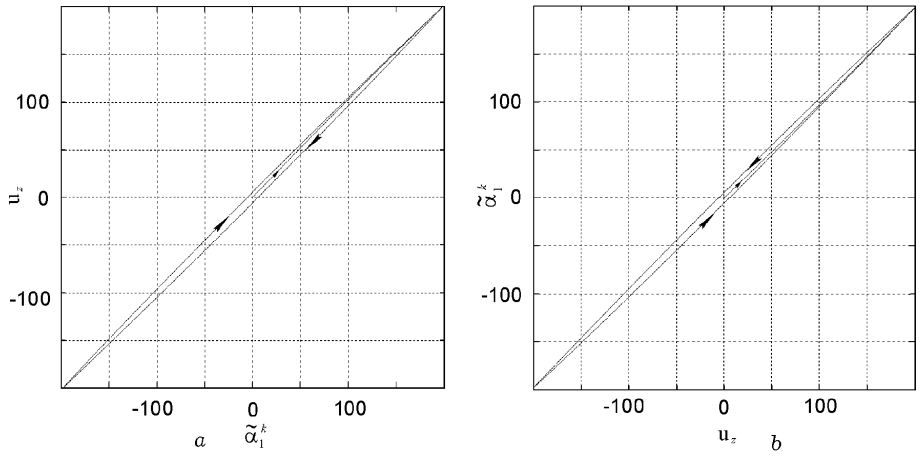

Figure 6. The hysteresis loops by $\mathcal{A}$ (a) and $\mathcal{B}$ (b) types of the piezo-drive static characteristics with parameters $m = 5.75$, $a_h = 2000$, $k = 1.9 \cdot 10^{-6}$, $p = 1.075$, $\tilde{p} = 5 \cdot 10^{-3}$ and $\alpha = 1.5$.

A *local function* $\tilde{x}_\nu(t)$ on each *local* time semi-interval $\mathrm{T}_\nu \equiv [t_\nu, t_{\nu+1})$ is introduced as

$$\tilde{x}_\nu(t) = x(t) - \check{x}_\nu \quad \forall t \in \mathrm{T}_\nu, \tag{5}$$

and a *nonlinear functionally-parametrized* coefficient $k_\nu \equiv k_\nu(x(t)) \equiv k_\nu(k, p, \tilde{p}, \tilde{x}_\nu)$ of the *hysteresis function shape* is defined as

$$k_\nu(x(t)) = k(1 - (1-p)\exp(-\tilde{p}|\tilde{x}_\nu|)),\ t \in \mathrm{T}_\nu, \tag{6}$$

where $k, p, \tilde{p}$ are constant positive parameters. For a constant parameter $\alpha_h > 0$ and $x_0 \equiv x(t_0)$ a *normed* hysteresis function $r(t) = \mathrm{Hst}(\cdot, x(t))$

$$\begin{aligned} r(t) &= \mathrm{Hst}(a_h, \alpha_h, k_\nu(x(t)), r_o, x(t)); \\ r(t_0) &\equiv r_o = \mathrm{Hst}(a_h, \alpha_h, k_\nu(x_0), r_o, x_0) \end{aligned} \tag{7}$$

with memory and restriction on its module by a constant parameter $a_h > 0$, is defined as a *right-sided* solution of the equations

$$\mathrm{D}^+ r = \begin{cases} k_\nu \left| r - a_h \mathrm{Sign}\, \dot{x}(t) \right|^{\alpha_h} \dot{x}(t) & |r| < a_h \\ 0 & |r| \geq a_h \end{cases}; \quad r(t_0 + 0) = r_o. \tag{8}$$

where D^+ is symbol of a *right derivative* with respect to a time. The differential equation in (8) has a *discontinuous* right side and *ambiquitely* depends on forcing function $x(t)$ and its speed $\dot{x}(t)$. Finally, at initial condition $y_o \equiv y_0 = y(t_0)$ for $x = x_0$ the hysteresis function $y(t)$ is defined in the form

$$y(t) \equiv m\, \mathrm{Hst}(a_h, \alpha_h, k_\nu, r_o, x(t)); \quad r_o \equiv y_o/m, \tag{9}$$

with the constant positive scale coefficient $m > 0$. In developed *differential* model (4)–(9) of physical hysteresis the parameter $\tilde{p}$ determines on the whole a *degree of convergence* (see Fig. 5) for a trajectory $y(t) = F_h(\cdot, x(t))$ in the plane $x\mathrm{O}y$ on symmetric *limiting static loop* under the harmonic forcing function $x(t) = A \sin \omega t$ with fixed A, ω and any initial condition $y_o = y_0$ with $|y_o|/m < a_h$. For this model all well-known requirements are realized, including the famous requirements on a model vibro-correctness (Krasnosel'skii and Pokrovskii, 1983), and also on a frequency independence and a fine return on a main symmetric limiting hysteresis loop after a short-term passage on a displaced local hysteresis loop (Palmov, 1976; Kochneva, 1979).

4.3 Static Model of the Piezo-drive Hysteresis

For contemporary piezo-ceramic materials their normed hysteresis not exceeds 5% for electric field strength $|E^e| \leq E^{em} = 2$ KV/cm. The PCE linear *normed* static characteristics is appeared as

$$\tilde{\alpha}_1^k \equiv \alpha_1^k / \mathrm{k}_u^\alpha = \mathrm{u}_z, \tag{10}$$

where

$$\mathrm{k}_u^\alpha \equiv -\frac{d_{31} l_p}{2\sqrt{2} \cdot h_p\, r_p\, \lambda_t^p} > 0,$$

l_p, r_p and $h_p \ll r_p$ are the PCE's length, mean radius and a wall thickness, the pure number

$$\lambda_t^p = \frac{1 - 2\sqrt{2}\, k_{31}^2/(3\pi) + (h_p/r_p)^2/12}{1 - k_{31}^2} > 1,$$

and $d_{31} < 0$ with $k_{31}^2 = d_{31}^2/(S_{11}^E \varepsilon_{33}^\sigma) < 1$ are standard notations of the piezo-ceramics' parameters (Smazhevskaya and Fel'dman, 1971).

At the the PCE's wall thickness $h_p = 1$ mm maximum voltage $\mathrm{u}_z^m = 200$ V corresponds to maximum of electric field strength $E_z^{em} = 2$ KV/cm. Fig. 6 presents some *experimental* (Somov and Fadeyev, 1980) results on the *normed* hysteresis characteristics by type

$\mathcal{A}$ ($\mathrm{u}_z = F_h(\cdot, \tilde{\alpha}_1^k)$, Fig. 6*a*) and by type $\mathcal{B}$ ($\tilde{\alpha}_1^k = \Phi_h(\cdot, \mathrm{u}_z)$, Fig. 6*b*) for this piezo-drive at input voltage $\mathrm{u}_z(t) = A \sin \omega t$ with $A = 200$ V and $\omega = 1$ rad/s. Moreover, there were carried out a statistic data processing and *preliminary* fitting the *hysteresis* parameters $m,\ a_h,\ \alpha,\ k,\ p,\ \tilde{p}$ taking into account the condition $m\,k\,p\,a_h^{\alpha} = 1$ for *initial* loading. In terms of *bending torques* the PCE's *static* hysteresis characteristic by the $\mathcal{A}$ type is presented in the form

$$\begin{gathered}(3E_q^p\, I_p/l_p)\, k_u^{\alpha}\, y(t) = \mathrm{k}_z^k\, \mathrm{u}_z(t);\\ y(t) = m\, r(t);\quad x(t) = \alpha_1^k(t)/k_u^{\alpha} = \tilde{\alpha}_1^k;\\ r(t) = \mathrm{Hst}(a_h, \alpha, k_\nu(x(t)), r_o, x(t)),\end{gathered} \tag{11}$$

with mandatory concordance of initial conditions

$$r_o = \mathrm{Hst}(a_h, \alpha, k_\nu(x_0), r_o, x_0),$$

where the constant coefficient

$$k_z^k = -\frac{3E_q^p I_p d_{31}}{2\sqrt{2}\, r_p \lambda_t^p h_p} \equiv -\frac{3(\pi/2)^5}{4\sqrt{2}} \left(\frac{r_p}{\lambda_t^p}\right)^2 \frac{d_{31}}{S_{11}^E},$$

and initial value $r_o = r(t_0) \equiv y_o/m = \mathrm{u}_z(t_0)/m$.

4.4 Dynamics of the Piezo-drive

If $w_y(t,x)$ is a transverse displacement any point at the PCE's axis, then $\alpha_1^k(t) = \partial w_y(t, l_p)/\partial x$ and a curvature $\kappa_z(E_z(t), x) = \partial^2 w_y(t,x)/\partial x^2$ of the PCE's bending in *linear* theory is appeared as

$$\kappa_z(E_z^e(t), x) = -[d_{31}/(\sqrt{2}\, r_p\, \lambda_t^p)]\; E_z^e(t), \tag{12}$$

where $E_z^e(t) = \mathrm{u}_z(t)/h_p$ is an electric field strength. For the PCE mass m_p, $m_p^l \equiv m_p/l_p$, $I_p \equiv \pi r_p^3 h_p$ and $E_e^p \equiv (S_{11}^E \lambda_t^p)^{-1}$ the well-known *wave equation*

$$m_p^l[\partial^2\, w_y(t,x)/\partial t^2] + I_p E_e^p\, [\partial^4\, w_y(t,x)/\partial x^4] = 0$$

without the PCE rotation inertia under standard boundary conditions have analytic solution. By *first* partial frequency $\Omega_1^p = (\pi/l_p)^2 (I_p E_e^p/m_p^l)^{1/2}$ of own PCE *bending* oscillations, the PCE have equivalent mass $m_e^p = (l_p/h_1^k)^2 m_p/32$, where h_1^k is a distance between the IMC mass center and point O, see Fig.4. For the IMC's mass m_1^k and moment of inertia J_1^k, the "IMC+PCE"-cluster have equivalent general mass $\mu_1^k \equiv J_1^k + (m_1^k + m_e^p)(h_1^k)^2$ in point O. For notations $E_q^p = (\pi/2)^4\ E_e^p/4$ and $c_1^k = 3E_q^p I_p/l_p \equiv \mu_1^k (\Omega_1^k)^2$ linear piezo-drive's dynamical model has the form

$$\begin{gathered}\mathrm{M}_1^{kr} + \mu_1^k(\ddot{\alpha}_1^k + \nu_1^k \Omega_1^k \dot{\alpha}_1^k + (\Omega_1^k)^2 \alpha_1^k) = \mathrm{Q}_1^k;\\ \mathrm{Q}_1^k \equiv 3E_q^p\, I_p\, \kappa_z(E_z^e(t), l_p)/2 = k_z^k\, \mathrm{u}_z(t),\end{gathered} \tag{13}$$

where $\mathrm{M}_1^{kr}(t)$ is an inertia torque because of a telescope motion. For its fixed position $\mathrm{M}_1^{kr} \equiv 0$, than taking into account the relations (10), (11), (12) and

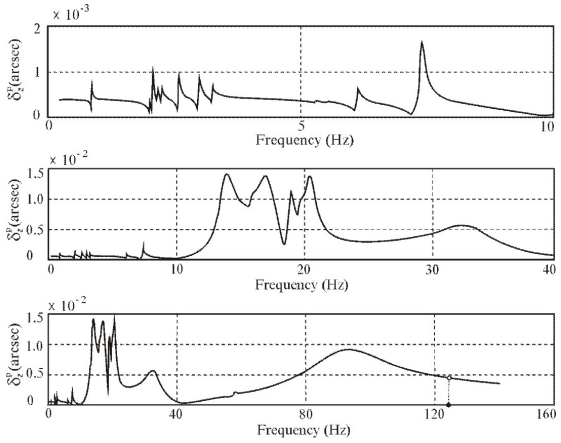

Figure 7. The vibration amplitude of the optical image

(13), the piezo-drive's dynamical *nonlinear hysteresis* model is appeared as

$$\begin{gathered}\mu_1^k[\ddot{\alpha}_1^k + \nu_1^k \Omega_1^k \dot{\alpha}_1^k + k_u^{\alpha}(\Omega_1^k)^2 y(t)] = k_z^k\, \mathrm{u}_z(t);\\ y(t) = mr(t);\, x(t) = \alpha_1^k/k_u^{\alpha};\, r(t) = \mathrm{Hst}(\cdot, x(t)),\end{gathered} \tag{14}$$

with concordance of initial conditions. The *final* parametric identification of the piezo-drive hysteresis is carried out by careful study of its nonlinear model (14) taking into account *experimental* data.

5 Vibrational Analysis of the Telescope

Some results on the vibrational analysis of the image motion $\delta_z^{\mathrm{p}}(t)$ onto the light detector while being subjected to the rotation frequency of all 6 statically unbalanced gyrodine's rotors in *ball bearings* and *without* a vibro-absorbing frame for the GMC fixation on the SC body, are given in Fig. 7. The vibration amplitude δ_z^{p} of this image at the gyro-rotor's nominal rotation frequency $\sim$ 125 Hz is equal to $\sim$ 0.005 arcsec. The use of the gyrorotor's 5-DOF *gas-dynamic* suspension in each gyrodine and placement of the GMC on the SC body by a *vibro-absorbing frame* made it possible a vibration amplitude of $\sim 0.2\,10^{-3}$ arcsec to be attained at this rotation frequency for all gyro-rotors.

6 Filtering and Robust Digital Control

As the main methods for synthesis of nonlinear control systems we use methods of *Lyapunov functions* and *vector Lyapunov functions* (VFL) in association with the *exact feedback linearization* (EFL) technique (Somov *et al.*, 1999). Contemporary filtering & alignment calibration algorithms (Somov, 2009) give finally a fine discrete estimating the SC angular motion coordinates by the quaternion $\mathbf{\Lambda}_s^{\mathrm{m}} = \mathbf{\Lambda}_s \circ \mathbf{\Lambda}_s^{\mathrm{n}}$, $s \in \mathbb{N}_0$, where $\mathbf{\Lambda}_s \equiv \mathbf{\Lambda}(t_s)$, $\mathbf{\Lambda}_s^{\mathrm{n}}$ is a "noise-drift" digital quaternion and a measurement period $T_q = t_{s+1} - t_s \le T_u$ is multiply with respect to a control period T_u.

In stage 1, for continuous forming the control torque $\mathbf{M}^{\mathbf{g}}(\boldsymbol{\beta}(t), \dot{\boldsymbol{\beta}}(t))$ (2) and the SC model as a free rigid

body the simplified controlled object is such:

$$\dot{\mathbf{\Lambda}}=\mathbf{\Lambda}\circ\boldsymbol{\omega}/2;\ \mathbf{J}\dot{\boldsymbol{\omega}}+[\boldsymbol{\omega}\times]\mathbf{G}^{o}=\mathbf{M}^{\mathbf{g}};\ \dot{\boldsymbol{\beta}}=\mathbf{u}^{\mathrm{g}}(t). \quad (15)$$

The error quaternion is $\mathbf{E}=(e_0,\mathbf{e})=\tilde{\mathbf{\Lambda}}^{p}(t)\circ\mathbf{\Lambda}$, Euler parameters' vector is $\boldsymbol{\mathcal{E}}=\{e_0,\mathbf{e}\}$, and the attitude error's matrix is $\mathbf{C}_e\equiv\mathbf{C}(\boldsymbol{\mathcal{E}})=\mathbf{I}_3-2[\mathbf{e}\times]\mathbf{Q}_e$, where $\mathbf{Q}_e\equiv\mathbf{Q}(\boldsymbol{\mathcal{E}})=\mathbf{I}_3e_0+[\mathbf{e}\times]$ with $\det(\mathbf{Q}_e)=e_0$. If error $\delta\boldsymbol{\omega}\equiv\tilde{\boldsymbol{\omega}}$ in the rate vector $\boldsymbol{\omega}$ is defined as $\tilde{\boldsymbol{\omega}}=\boldsymbol{\omega}-\mathbf{C}_e\boldsymbol{\omega}^{p}(t)$, and the GMC's required control torque vector $\mathbf{M}^{\mathbf{g}}$ is formed as $\mathbf{M}^{\mathbf{g}}=\boldsymbol{\omega}\times\mathbf{G}^{o}+\mathbf{J}(\mathbf{C}_e\dot{\boldsymbol{\omega}}^{p}(t)-[\boldsymbol{\omega}\times]\mathbf{C}_e\boldsymbol{\omega}^{p}(t)+\tilde{\mathbf{m}})$, then the simplest nonlinear model of the SC's attitude error is as follows:

$$\dot{e}_0=-\langle\mathbf{e},\tilde{\boldsymbol{\omega}}\rangle/2;\ \ \dot{\mathbf{e}}=\mathbf{Q}_e\tilde{\boldsymbol{\omega}}/2;\ \ \dot{\tilde{\boldsymbol{\omega}}}=\tilde{\mathbf{m}}. \quad (16)$$

For model (16) a *non-local nonlinear* coordinate transformation is defined and applied at analytical synthesis by the EFL technique. This results in the nonlinear CL

$$\tilde{\mathbf{m}}(\boldsymbol{\mathcal{E}},\tilde{\boldsymbol{\omega}})=-\mathbf{A}_0\,\mathbf{e}\,\mathrm{sgn}(e_0)-\mathbf{A}_1\,\tilde{\boldsymbol{\omega}}, \quad (17)$$

where $\mathbf{A}_0=((2a_0^{*}-\tilde{\omega}^2/2)/e_0)\mathbf{I}_3$; $\mathbf{A}_1=a_1^{*}\mathbf{I}_3-\mathbf{R}_{e\omega}$, $\mathrm{sgn}(e_0)=(1,\text{ if }e_0\geq 0)\vee(-1,\text{ if }e_0<0)$, matrix $\mathbf{R}_{e\omega}=\langle\mathbf{e},\tilde{\boldsymbol{\omega}}\rangle\mathbf{Q}_e^{\mathrm{t}}[\mathbf{e}\times]/(2e_0)$, and parameters a_0^{*},a_1^{*} are analytically calculated on spectrum $\mathrm{S}_{ci}^{*}=-\alpha_c\pm j\omega_c$. Simultaneously the VFL $\boldsymbol{\upsilon}(\boldsymbol{\mathcal{E}},\tilde{\boldsymbol{\omega}})$ is analytically constructed for close-loop system (16) and (17). Into orthogonal canonical basis Oxyz, see Fig. 3, the GD's AM units have next projections: $x_1=C_1$; $x_2=C_2$; $y_1=S_1$; $y_2=S_2$; $x_3=S_3$; $x_4=S_4$; $z_3=C_3$; $z_4=C_4$; $y_5=C_5$; $y_6=C_6$; $z_5=S_5$; $z_6=S_6$, where $S_p\equiv\sin\beta_p$ and $C_p\equiv\cos\beta_p$. Than column of normed GMC's summary AM vector $\mathbf{h}(\boldsymbol{\beta})=\{\mathsf{x},\mathsf{y},\mathsf{z}\}=\{\Sigma x_p,\Sigma y_p,\Sigma z_p\}$ and matrix $\mathbf{A}_{\mathrm{h}}(\boldsymbol{\beta})=\partial\mathbf{h}/\partial\boldsymbol{\beta}$ has the form

$$\mathbf{A}_{\mathrm{h}}(\boldsymbol{\beta})=\begin{bmatrix}-y_1 & -y_2 & z_3 & z_4 & 0 & 0\\ x_1 & x_2 & 0 & 0 & -z_5 & -z_6\\ 0 & 0 & -x_3 & -x_4 & y_5 & y_6\end{bmatrix}.$$

For *3-SPE* scheme singular state is appeared when the matrix Gramme $\mathbf{G}(\boldsymbol{\beta})=\mathbf{A}_h(\boldsymbol{\beta})\mathbf{A}_h^{\mathrm{t}}(\boldsymbol{\beta})$ loses its full rang, e.g. when $\mathsf{G}\equiv\det\mathbf{G}(\boldsymbol{\beta})=0$. At introducing the denotations

$$x_{12}=x_1+x_2;\ \ x_{34}=x_3+x_4;\ \ y_{12}=y_1+y_2;$$
$$y_{56}=y_5+y_6;\ \ \ z_{34}=z_3+z_4;\ \ z_{56}=z_5+z_6;$$
$$\tilde{x}_{12}=x_{12}/\sqrt{4-y_{12}^2}\,;\ \tilde{x}_{34}=x_{34}/\sqrt{4-z_{34}^2};$$
$$\tilde{y}_{12}=y_{12}/\sqrt{4-x_{12}^2}\,;\ \ \tilde{y}_{56}=y_{56}/\sqrt{4-z_{56}^2};$$
$$\tilde{z}_{34}=z_{34}/\sqrt{4-x_{34}^2}\,;\ \ \ \tilde{z}_{56}=z_{56}/\sqrt{4-y_{56}^2}$$

components of the GMC explicit vector tuning law

$$\mathbf{f}_{\rho}(\boldsymbol{\beta})\equiv\{f_{\rho1}(\boldsymbol{\beta}),f_{\rho2}(\boldsymbol{\beta}),f_{\rho3}(\boldsymbol{\beta})\}=\mathbf{0} \quad (18)$$

are applied in the form

$$f_{\rho1}(\boldsymbol{\beta})\equiv\tilde{x}_{12}-\tilde{x}_{34}+\rho\,(\tilde{x}_{12}\,\tilde{x}_{34}-1);$$
$$f_{\rho2}(\boldsymbol{\beta})\equiv\tilde{y}_{56}-\tilde{y}_{12}+\rho\,(\tilde{y}_{56}\,\tilde{y}_{12}-1);$$
$$f_{\rho3}(\boldsymbol{\beta})\equiv\tilde{z}_{34}-\tilde{z}_{56}+\rho\,(\tilde{z}_{34}\,\tilde{z}_{56}-1).$$

The analytical proof have been elaborated that vector tuning law (18) ensures absent of singular states by this GMC scheme for all values of the GMC AM vector $\mathbf{h}(t)\in\mathbf{S}\setminus\mathbf{S}^{*}$, i.e. inside all its variation domain.

Discrete measured error quaternion and Euler parameters' vector are $\mathbf{E}_s=(e_{0s},\mathbf{e}_s)=\tilde{\mathbf{\Lambda}}^{p}(t_s)\circ\mathbf{\Lambda}_s^{\mathrm{m}}$ and $\boldsymbol{\mathcal{E}}_s=\{e_{0s},\mathbf{e}_s\}$, and the attitude error filtering is executed by the relations

$$\tilde{\mathbf{x}}_{s+1}=\tilde{\mathbf{A}}\tilde{\mathbf{x}}_s+\tilde{\mathbf{B}}\mathbf{e}_s;\mathbf{e}_s^{\mathrm{f}}=\tilde{\mathbf{C}}\tilde{\mathbf{x}}_s+\tilde{\mathbf{D}}\mathbf{e}_s, \quad (19)$$

where matrices $\tilde{\mathbf{A}},\tilde{\mathbf{B}},\tilde{\mathbf{C}}$ and $\tilde{\mathbf{D}}$ have conforming dimensions and some general turning parameters. Attitude filtered error vector $\mathbf{e}_k^{\mathrm{f}}$ is applied for forming the digital control $\tilde{\mathbf{m}}_k=\mathbf{u}_k$ taking into account a time delay at incomplete measurement of state and onboard signal processing:

$$\mathbf{v}_k=-(\mathbf{K}_{\mathrm{d}}^{\mathrm{x}}\,\hat{\mathbf{x}}_k+\mathbf{K}_{\mathrm{d}}^{\mathrm{u}}\,\mathbf{u}_k);\ \ \mathbf{u}_{k+1}=\mathbf{v}_k; \quad (20)$$

$$\hat{\mathbf{x}}_{k+1}=\mathbf{A}_{\mathrm{od}}\,\hat{\mathbf{x}}_k+\mathbf{B}_{\mathrm{od}}^{\mathrm{u}}\,\mathbf{u}_k+\mathbf{B}_{\mathrm{od}}^{\mathrm{v}}\,\mathbf{v}_k$$
$$+\mathbf{G}_{\mathrm{d}}(\mathbf{e}_k^{\mathrm{f}}-(\mathbf{C}_{\mathrm{od}}\,\hat{\mathbf{x}}_k+\mathbf{D}_{\mathrm{od}}^{\mathrm{u}}\,\mathbf{u}_k+\mathbf{D}_{\mathrm{od}}^{\mathrm{v}}\,\mathbf{v}_k)),$$

where $\hat{\mathbf{x}}_k=\{\hat{\mathbf{e}}_k,\hat{\tilde{\boldsymbol{\omega}}}_k\}$, matrices have conforming dimensions and also general *turning parameters* to guarantee the ACS robust properties.

In stage 2, the problems of synthesising the digital nonlinear CL were solved for model of the flexible spacecraft (1) with incomplete discrete measurement of state. Furthermore, the selection of parameters in the structure of the GMC nonlinear robust CL which optimizes the main quality criterion for given restrictions, including coupling and damping the SC structure oscillations (Somov *et al.*, 2005) is fulfilled by a parametric optimization and multistage numerical simulation. Thereto, the VLF has the structure derived above for the error coordinates $\boldsymbol{\mathcal{E}},\tilde{\boldsymbol{\omega}}$ and the structure of other VLF components in the form of *sub-linear norms* for vector variables $\mathbf{q}(t)$, $\dot{\mathbf{q}}(t)$, $\dot{\boldsymbol{\beta}}(t)$ using the vector $\boldsymbol{\beta}(t)$. For attitude stabilization of a space telescope body by the *ATLAST*-8m class there are needed a control period $T_u=4$ s and a measurement period $T_q=1$ s. As far as the ACS II cascade is concerned, here standard digital PID-controllers are applied with a control period $T_u=0.125$ s and a measurement & filtering period $T_q=T_u/4$.

7 Computer Simulation

Suggested two-cascaded nonius control system was simulated with approximate data for a space telescope by the *ATLAST*-8m class. Most interest results are presented in Fig. 8 — angular velocity error $\dot{\delta}_z^{\mathrm{p}}(t)$ in the

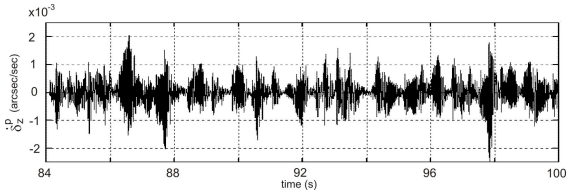

Figure 8. Angular velocity error on the light detector when operating the image-motion stabilization system

light detector of the telescope for time interval of a steady-state mode with operating II cascade. Here the *mean-square error* $\sigma = 0.4567\,10^{-3}$ arcsec/sec was obtained for the angular velocity error $\dot{\delta}_z^{\rm p}(t) \quad \forall t \in [84, 100]$ s.

8 Conclusion

Some problems on a guidance, robust attitude control and long-time image motion stabilization of a large space astronomical telescope by the *ATLAST*-8m class were considered.

Two-cascaded nonius control system was suggested which in cooperation with the solar pressure balancing system by the SAPs slow angular replacements for permanent unloading an accumulated AM of the GMC may be applied for a long-time ultra-precise image motion stabilization.

Elaborated methods for dynamic research at external and parametric disturbances, partial discrete measurement of the state, digital control of the gyro moment cluster and a fine piezo-driver, and also some results of computer simulation, were presented.

Acknowledgements

The work was supported by Russian Found for Basic Research (RFBR, Grant 11-08-01037) and by Division on EMMCP of the Russian Academy of Sciences (Program for Basic Research no. 15, project 1.3 via Samara Scientific Center, Russian Academy of Sciences).

References

Crenshaw, J.W. (1973). 2-SPEED, a single-gimbal control moment gyro attitude control systems. *AIAA Paper* (73-895), 1–10.

Dahl, P.R. (1968). *A Solid Friction Model. Report TOR-158(3107-18)*. El Segundo, CA, USA.

Dahl, P.R. (1976). Solid friction damping of mechanical vibrations. *AAAI Journal* **14**(12), 1675–1682.

Haessing, D.A. and B. Friedland (1991). On the modeling and simulation of friction. *ASME Journal of Dynamic Systems, Measurement and Control* **113**(3), 354–362.

Hopkins, R.C., P. Capizzo, S. Fincher and et al. (2010). Spacecraft conceptual design for the 8-meter Advanced Technology Large Aperture Space Telescope *ATLAST*. Technical Report M10-0765. NASA Marshall Space Flight Center.

Karnopp, D. (1985). Computer simulation of stricksliip friction in mechanical dynamic systems. *ASME Journal of Dynamic Systems, Measurement and Control* **107**(1), 100–103.

Kochneva, L.F. (1979). *Internal Friction in Solid Bodies at Oscillations*. Nauka. Moscow.

Krasnosel'skii, M.A. and A.V. Pokrovskii (1983). *Systems with a Hysteresis*. Nauka. Moscow.

Palmov, V.A. (1976). *Oscillations of Elastico-plastic Bodies*. Nauka. Moscow.

Panovko, Ya.G. (1960). *Internal Friction at Oscillations of Flexible Systems*. FizMatGiz. Moscow.

Pisarenko, G.S. (1970). *Oscillations of Mechanical Systems with regard for an imperfect flexibility of materials*. Naukova Dumka. Kiev.

Postmant, M., T. Brown, A. Koekemoer, M. Giavalisco and et al. (2008). Science with an 8-meter to 16-meter optical/UV space telescope. In: *Proceedings of the SPIE*. Vol. 7010. pp. 701021–701032.

Smazhevskaya, E.G. and N.B. Fel'dman (1971). *Piezoelectric Ceramics*. Soviet Radio. Moscow.

Somov, Ye. (2009). Multiple algorithms for filtration, integration and calibration of a strapdown inertial system for a spacecraft attitude determination. In: *Proceedings of 16th Saint Petersburg International Conference on integrated navigation systems*. Saint Petersburg. pp. 110 –112.

Somov, Ye., S. Butyrin and S. Somov (2005). Coupling and damping the structure oscillations at spacecraft gyromoment digital control. In: *Proceedings of the IEEE/EPS International Conference on Physics and Control*. pp. 497–502. Saint Petersburg.

Somov, Ye., S. Butyrin, V. Matrosov and et al. (1999). Ultra-precision attitude control of a large low-orbital space telescope. *Control Engineering Practice* **7**(9), 1127–1142.

Somov, Ye.I. (1974). *The device for a ray deflection. The USSR Patent* 543301.

Somov, Ye.I. (2000). Model of phisical hysteresis and control of the image motion oscillations at a large space telescope. In: *Proceedings of 2nd International Conference COC'2000*. Vol. 1. St.Petersburg. pp. 70–75.

Somov, Ye.I. and A.A. Fadeyev (1980). Some construction solutions, static and dynamic characteristics of control devices at the precise image stabilization systems. In: *Dynamics of Spacecraft Control*. pp. 204–216. Institute for Theoretical and Applied Mechanics, the Siberian Branch of RAS. Novosibirsk.

Somov, Ye.I. and L.Z. Dul'kin (1975). *The astronomical telescope with the precise stabilization of an image position. The USSR Patent* 558595.

Sorokin, E.S. (1960). *On Internal Friction Theory at Oscillations of Flexible Systems*. GosStroyIzdat. Moscow.